ELSEVIER

Polymer 42 (2001) 6231–6237

polymer

www.elsevier.nl/locate/polymer

Lamellar twisting in α isotactic polypropylene transcrystallinity investigated by synchrotron microbeam X-ray diffraction

E. Assouline[a,b,*], E. Wachtel[c], S. Grigull[d], A. Lustiger[e], H.D. Wagner[b], G. Marom[a]

[a]*Casali Institute of Applied Chemistry, Edmond Safra Campus, Givat Ram, The Hebrew University of Jerusalem, Jerusalem 91904, Israel*
[b]*Department of Materials and Interfaces, The Weizmann Institute of Science, Rehovot 76100, Israel*
[c]*Chemical Services Unit, The Weizmann Institute of Science, Rehovot 76100, Israel*
[d]*ESRF, BP 220, F-38043 Grenoble Cedex, France*
[e]*ExxonMobil Research and Engineering, Route 22 East, Annandale, NJ 08801, USA*

Received 17 October 2000; received in revised form 21 December 2000; accepted 22 January 2001

Abstract

We report for the first time details of the morphology of α isotactic polypropylene transcrystallinity induced by aramid fibers as determined by high spatial resolution X-ray diffraction. We suggest that the parent lamellae nucleate at the fiber surface with the crystallite *c*-axes parallel to the fiber axis, twist one quarter turn about the parent a^*-axis within an approximate distance of 25 μm and then continue to grow without further twisting. This result is unexpected since lamellar twisting has never been observed in pure α spherulitic polypropylene.

Keywords: Polypropylene; α Transcrystallinity; Lamellar twisting

1. Introduction

Fibers inserted in a semi-crystalline polymer matrix may nucleate and induce a crystalline morphology at their surface, which is different from the one in the bulk: the transcrystalline (tc) layer. The crystallite orientation within the tc layer depends on the nature of the matrix [1–3] and may vary with distance from the fiber. For instance, it was inferred from the study of carbon and aramid fiber reinforced nylon 66 [1] that there are two main conformations in the tc layer. Close to the fiber surface, the nylon chain axes — the *c*-axes of the crystallites — are parallel to the fiber. Further from the fiber, the *c*-axes of the crystallites are perpendicular to the fiber due to a probable sheaf-like structure of the lamellae. In polyethylene/polyethylene composites [2], it was concluded that the *c*-axes of the crystallites in the interfacial layer near the surface of the fiber are aligned with the fiber and that the lamellae twist as the crystallites grow outwards from the fiber. The thickness of such an oriented layer surrounding each fiber may affect the mechanical properties of the whole composite [4]. Transcrystallization of isotactic polypropylene (iPP) in fiber-reinforced composites is particularly interesting since there are three different crystalline polymorphs, α, β and γ. The α monoclinic structure, obtained in the absence of any special treatment, is unique regarding its crystallization process since secondary lamellae (daughters) grow epitaxially on the *ac* faces of the primary lamellae (parents) [5,6]. The β hexagonal iPP tc layer is generated either by coating the fiber with a specific nucleating agent [7] or by exerting a shearing stress at the fiber during the cooling [8]. The γ orthorhombic transcrystallinity [9] is less common and is obtained under high pressure.

Here, we focus on the detailed morphology of the α iPP tc layer. Three models which have already been published in the literature present significant differences among themselves. The first, regarding treated glass fiber reinforced iPP [7], was deduced from scanning electron microscopy (SEM) observations. It considered only one population of lamellae for which the chain axis is parallel to the fiber. Another was based on micromechanical measurements in high modulus carbon/iPP [10] composites. It also refers to one type of lamellae but the *c*-axis was shown to be in the equatorial plane. The last, concerning iPP composites, reinforced with either Kevlar 29 or high modulus carbon fibers, [11] takes into account the presence of both parent and daughter lamellae. In this model, which was based on X-ray diffraction data, the *c*-axes of the crystallites in the parent lamellae are parallel to the fiber. Yet, it considers

* Corresponding author. Fax: +972-2-658-60-68.
E-mail address: eric@vms.huji.ac.il (E. Assouline).

0032-3861/01/$ - see front matter
PII: S0032-3861(01)00087-8

only the case of composites with high volume fraction of fibers. In the present paper, we reconcile the differences among the various reports in the literature, and develop a fully consistent model of α iPP which takes into account the presence of both types of lamellae and which shows that the occurrence of a particular orientation of these lamellae depends on the measurement position relative to the fiber.

2. Experimental section

2.1. Sample preparation

A thin film of α isotactic polypropylene (provided by Exxon, $MFR = 12$, $M_n = 43,600$ and $M_w = 212,500$) was crystallized on parallel and equidistant aramid fibers (Kevlar 149, DuPont, 12 μm diameter). The device used for positioning the fibers is described in Ref. [12]. The thickness of the film varied from 20 to 200 μm and was adjusted to match the interfiber distance. Using the temperature-controlled Mettler FP80, the hot-stage temperature was raised to 204°C over a period of 3 min to erase the previous thermal history of the sample. A fast cooling (−20°C/min) enabled us to reach the isothermal crystallization temperature (in the range 128–139°C). A Nikon optical microscope equipped with crossed polarizers permitted viewing the inner cell of the Mettler FP82 hot stage. The sample was removed from the furnace when transcrystallinity filled the whole interfiber space and was quenched. This thermal treatment resulted in the subsequent appearance of very small spherulites (diameter below 10 μm) in the bulk matrix as may be seen in Fig. 1 of Ref. [9].

2.2. Scanning electron microscopy

The composites were cross-sectioned with a razor blade so that the ends of the fibers would be exposed. In this way, details of transcrystallinity at and perpendicular to the film surface could be examined. The samples were etched according to the method of Bassett and Olley [13] by placing them in an Erlenmeyer flask containing a 0.7% w/v solution of potassium permanganate in a 2:1 sulfuric acid/orthophosphoric acid mixture and stirred vigorously for 15 min. They were then removed from the solution and washed with 30% hydrogen peroxide followed by water for about one minute each. Samples were coated with a thin (20 Å) coating of chromium before observation in the JEOL Field Emission SEM, operated at 3.0 kV accelerating voltage.

2.3. Laboratory wide angle X-ray diffraction

X-ray diffraction patterns were obtained on Fuji imaging plates, using a Searle camera equipped with Franks optics affixed to an Eliott GX6 rotating anode generator operating at 1.2 kW and producing copper radiation. The X-ray beam was nickel filtered ($\lambda = 1.54$ Å) and was about 400 μm in diameter in the plane of the sample. The exposure time was between 2 — for thinner samples — and 6 h — for thicker composites. The imaging plates were scanned with a helium-neon laser (Spectra Physics) in conjunction with a home-made reader based on an Optronics (Chelmsford, MA) densitometer and interfaced to a computer.

2.4. Synchrotron wide angle X-ray diffraction

The X-ray beam at the ID11 beamline of the European Synchrotron Radiation Facility (ESRF) was monochromatized ($\lambda = 0.25$ Å) and focused with a Laue crystal to 8 μm in the direction normal to the fibers and confined by a slit to 40 μm in the direction parallel to the fiber. The exposure time was 30 s. The data were collected using a tapered-optics CCD camera (Medoptics, Tucson, AZ) with a pixel size 50×50 μm^2.

2.5. Analysis of the X-ray diffraction patterns

The images were processed using the public domain NIH or ImageJ image processing programs, both available on zippy.nimh.nih.gov. The histograms of the angular distribution of intensity around the diffraction rings were calculated using home-made software and fitted using Origin 4.1. (Microcal, Northampton, MA). The measured azimuthal angles δ were corrected, when necessary, using the Eq. (1) [14]:

$$\cos\phi = \cos\theta\cos\delta, \tag{1}$$

where δ is the Bragg angle and φ is the angle which the reciprocal lattice makes with the fiber axis.

3. Results

3.1. Low spatial resolution X-ray diffraction

Using the laboratory source, two types of X-ray diffraction patterns of transcrystallinity were obtained. In both

Table 1
Indexing of the X-ray diffraction pattern of α iPP transcrystallinity (from Figs. 1 and 2)

Reflection	Experimental 2θ (°)	Experimental d (Å)	Literature d (Å) [15]	hkl[a]
1	14.12	6.27	6.26	110
2	16.91	5.24	5.23	040
3	18.61	4.77	4.78	130
4	21.38	4.16	4.16	111
5	21.92	4.06	4.05	041
6	25.50	3.49	3.49	060
7	28.47	3.13	3.13	220

[a] The indexing is based on the monoclinic lattice with $a = 6.65$ Å, $b = 20.96$ Å, $c = 6.50$ Å and $\beta = 99°20'$. The dimensions of the unit cell in reciprocal space are $a^* = 0.1524$ Å^{-1}, $b^* = 0.0477$ Å^{-1}, $c^* = 0.1559$ Å^{-1} and $\beta^* = 80°40'$.

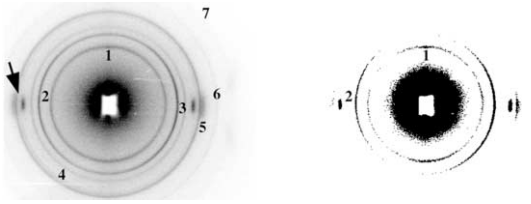

Fig. 1. (a) X-ray pattern of α iPP transcrystallinity in samples where the distance between the surfaces of the fibers is about 10 μm. The X-ray beam is perpendicular to the plane of the sample and has a cross-sectional area of about $400 \times 400\ \mu m^2$. Part of the X-ray pattern of the vertically oriented aramid fibers is indicated by the arrow; (b) X-ray pattern of α iPP transcrystallinity in the same sample after adjusting the contrast in order to emphasize the presence of 4 arcs in the (110) reflection. In both pictures, the numbering refers to Table 1.

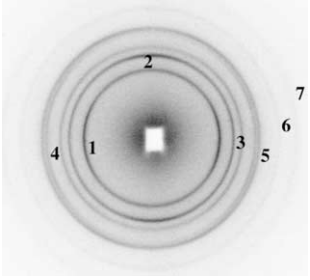

Fig. 2. X-ray pattern of α iPP transcrystallinity in samples where the distance between the fibers is in the range 50–200 μm. The experimental arrangement is as for Fig. 1. Fiber direction vertical. The numbering refers to Table 1.

cases the ring indexing is consistent with the α polymorph of isotactic polypropylene (Table 1). In samples where the distance between the surfaces of the fibers is approximately 10 μm, the X-ray pattern (Fig. 1) is similar to the one presented by Dean et al. [11]. The (110) reflection consists of 4 arcs: the two equatorial arcs appear weaker than the two meridional ones. From these data, two populations of lamellae can be identified: one where the a^*-axes of the crystallites are in the equatorial plane and one where the *a*-axes are parallel to the fiber. The (040) reflection is clearly equatorial; since there are only two arcs, the *b*-axes are in the equatorial plane for both populations. In fiber-reinforced composites where the distance between the surfaces of the fibers is larger — in the range 50–200 μm — a significantly different X-ray pattern (Fig. 2) is obtained. The (110) reflection contains only near equatorial intensity and the (040) reflection is meridional. These results were reproduced with Kevlar 29 reinforcing fibers, with MFR 34 and Achieve 3825 polypropylene, and with different crystallization temperatures.

3.2. SEM

The SEM picture (Fig. 3) displays the cylindrical shape of the tc layer. It shows clearly that the tc layer fills the whole interfiber space and that the growth front is parallel to the fiber axis. The widths of the striations look similar in the two perpendicular planes of the tc layer despite the fact that the two dimensions of the lamellae perpendicular to the growth direction are expected to be significantly different.

Fig. 3. Scanning electron micrograph of the α iPP tc layer. The arrows indicate the location of the fibers. The arrow heads stress the cylindrical shape of the tc layers.

3.3. High spatial resolution X-ray diffraction

In order to resolve the apparent contradiction between the two sets of X-ray diffraction measurements described above, we used the finely collimated synchrotron beam. It allowed us to scan the tc layer in the radial direction from the fiber surface to the bulk. Fig. 4 displays the X-ray patterns of the tc layer sampled at 8 μm intervals beginning near the fiber surface. The tc layer is always monoclinic (the ring indexing is as reported in Table 1) but the positions of the centers of the arcs reveal a progressive change of the orientation of the crystallites as a function of the distance from the fiber. Very close to the fiber (Fig. 4a), the (110) reflection consists of two meridional arcs whereas the (040) arcs are equatorial. In Fig. 4b–e, it is clearly seen that the (110) arcs rotate from the meridian to the equatorial plane while the (040) arcs rotate from the equatorial plane to the meridian (Table 2). The rotation of these reciprocal lattice

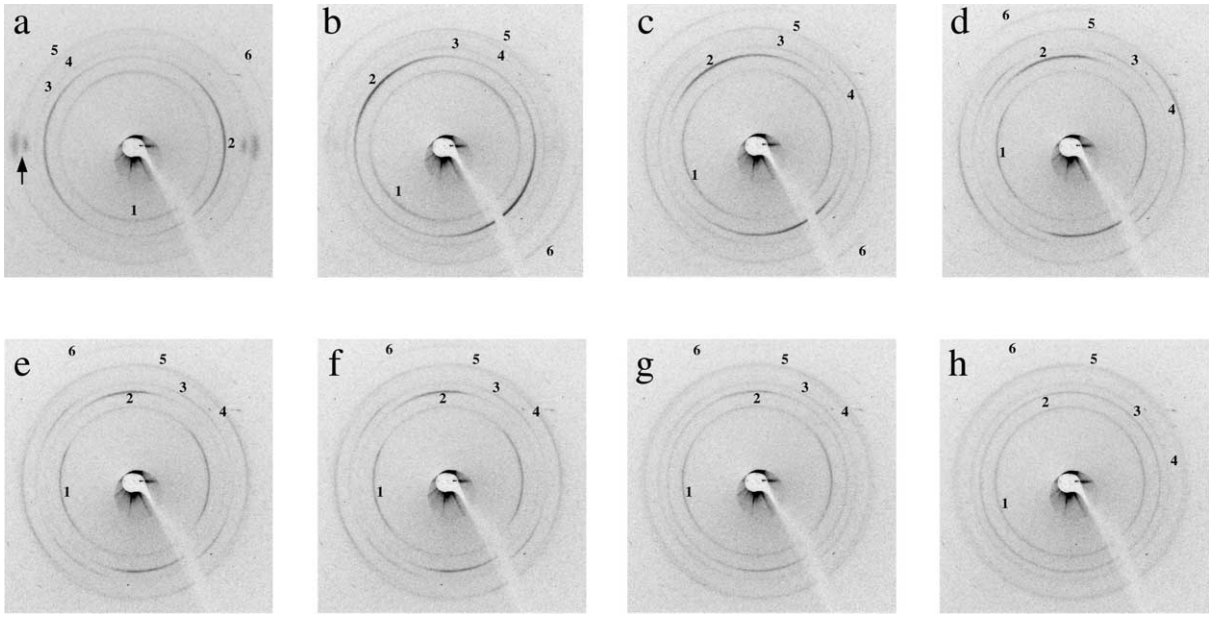

Fig. 4. X-ray patterns of iPP transcrystallinity (a) initial position: near the fiber surface (the arrow denotes the presence of the diffraction arcs of the aramid fibers); (b) 8 μm from the initial position; (c) 16 μm from the initial position; (d) 24 μm from the initial position; (e) 32 μm from the initial position; (f) 40 μm from the initial position; (g) 48 μm from the initial position; (h) 56 μm from the initial position. Fiber direction vertical. The X-ray beam is perpendicular to the plane of the sample and has a cross-sectional area of about 8×40 μm^2. In all the pictures, the numbering refers to Table 1.

vectors as a function of the distance from the fiber surface is not uniform. In Fig. 4e–g, the X-ray pattern remains unchanged: the rotation of the reciprocal lattice vectors saturates at large distance from the fiber. In Fig. 4h, which was measured at approximately 56 μm from the fiber, the pattern consists of full, uniform intensity rings. This isotropic pattern is consistent with the presence of small spherulites. As was discussed in Section 2 the cross-sectional area of the X-ray beam is larger than a spherulite thereby allowing the averaging over all lamellar orientations.

4. Discussion

4.1. Lamellar twisting model

The X-ray diffraction patterns of Fig. 4a and Fig. 1 are similar. Apparently, the transcrystallinity close to the fiber surface has the same morphology as in samples where the fiber surfaces are spaced at a distance of approximately 10 μm from each other. In both patterns, the (040) arcs are equatorial and meridional arcs are found for (110). The main difference is that the (110) reflection in Fig. 4a does not include any equatorial arcs (see comments below). The higher angle reflections in Fig. 4a are weak and cannot contribute to the analysis. However the two innermost reflections provide sufficient information to develop a model, since they allow one to deduce the orientation of two of the three crystallite axes.

Table 2
Azimuthal position (°) of the maximum of diffracted intensity (*hkl*) with respect to the fiber axis as a function of the distance of the sample area from the fiber (from Fig. 4). The angles were measured on the histogram, calculated from the upper half of the patterns

hkl	0	8 μm	16 μm	24 μm	32 μm	40 μm	48 μm
110	0	40	68	79	85	85	85
040	90	49	23	11	6	6	6

The morphology of α iPP transcrystallinity close to the fiber surface can be described by a model similar to the one developed by Dean et al. [11] (Fig. 5a). As mentioned earlier, two populations of lamellae are expected, i.e. the parent and the daughter lamellae. The growth of the daughter lamellae is initiated on the lateral *ac* faces of the parent lamellae [6]. The angle between the two populations is 80°40′ [5]. The orientation of parent lamellae is deduced from the (110) arcs which are equatorial. Thus the *c*-axes of the crystallites in parent lamellae are parallel to the fiber. The a^*-axes (which are the growth axes) and the *b*-axes are in the equatorial plane. The data presented in Table 3 are consistent with this result since all the intensity maxima of the X-ray diffraction arcs (*hk*0) are in the plane perpendicular to the fiber. The absence of equatorial (110) arcs can now be explained: due to the small width of the synchrotron beam, when the beam is focused at the fiber, relatively few parent crystallites will be oriented properly for the (110) reciprocal lattice vector to intersect the Ewald sphere. The orientation of the daughter lamellae is deduced from the (110) arcs that are almost meridional. Four arcs are expected (see Table 3) but since they are close to the meridian and the

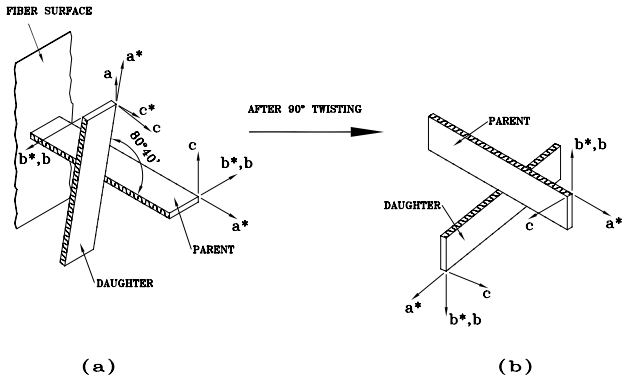

Fig. 5. An idealized model of the α iPP transcrystallinity, (a) close to the fiber; (b) further than 25 μm from the fiber. The monoclinic unit cell axes are defined in the footnote to Table 1. Other symmetrically related daughter lamellae grow on the parent lamella; however, in the interest of clarity, we have drawn only one daughter lamella.

orientational distribution is broad, only two broad unresolved peaks were observed. The *a*-axes of the crystallites in the daughter lamellae are parallel to the fiber. The positions of the *b*- and *c*-axes are fixed by the relative orientation of daughter lamellae with respect to parent lamellae as observed in spherulitic iPP [5]. Although the outer arcs corresponding to the daughter lamellae are weak in our pictures due to the short exposure time (Figs. 1 and 4a), the calculated angular positions of the center of the arcs with respect to the fiber are consistent with the measured ones in the work of Dean et al. [11].

Beginning with the model of Fig. 5a, only a rotation around the parent a^*-axis (which is parallel to the daughter c^*-axis) can explain the position of the arcs in Fig. 4b–e. Regarding the daughter lamellae, this rotation causes the *a*-axis to move towards the equatorial plane, whereas the b^*-axis rotates towards the fiber axis. Thus, since the value of b^* is much smaller than that of a^*, the (110) arcs move from the nearly meridional position towards the equatorial plane. On the other hand, the (040) arcs move from the equator to the meridian (for both the parent and daughter lamellae). The (110) arcs due to the parent lamellae would move only from the equatorial plane to a nearly equatorial plane. Thus, the reflections due to the parent lamellae overlap those of the daughter lamellae. At this stage the patterns of the parent and daughter lamellae are similar, as shown in Table 4, which presents the predicted and measured angles of all the arcs for the two types of lamellae. Beyond approximately 25 μm from the fiber surface, the lamellae remain in this conformation. The parent lamellae grow radially with the a^*-axis as the growth direction. This is consistent with the microscopy observation: the growth front is parallel to the fiber (Fig. 3). The apparent discrepancy among the literature results can now be resolved. On the one hand, samples with small interfiber distance (Fig. 1), i.e. high volume fraction of fibers, induce the conformation close to the fiber characterized by Fig. 4a. On the other hand, samples with large interfiber distance generated an X-ray pattern (Fig. 2) similar to Fig. 4e–g. Here, the model resembles the one presented on the basis of micromechanical considerations [10] but also takes into account the presence of daughter lamellae. It should be noted that in the pattern presented in Fig. 2, the diffraction signal is dominated by the transcrystalline areas that are distant from the fiber since the volume they occupy is much larger than that of the transcrystalline zones close to the fiber. In this case, the *b*-axes are parallel to the fiber, the *c*-axes and the a^*-axes are all perpendicular to the fiber. This model, presented in Fig. 5b, is fully consistent with a 90° rotation of the model displayed in Fig. 5a around the parent a^*-axis. It should be noted that the rotation was somewhat short of 90° in the ESRF experiments (Fig. 4e–g).

4.2. Is the lamellar twist model unique?

In view of the data presented above, it is clear that the

Table 3
Calculated and measured azimuthal angles of the maximum of diffracted intensity (*hkl*) with respect to the fiber axis, close to the fiber surface. The measurements were made on the histograms calculated from Fig.1 and from the upper half of Fig. 4a. The calculation was based on the lamellar twist model described in the text and in Fig. 5a

	Parent lamellae		Daughter lamellae	
hkl	Calculated angle (°)	Measured angle (°)	Calculated angle (°)	Measured angle (°)
110	90	90[a]	19.7	~0[a,b,c]
040	90	90[a,b]	90	90[a,b]
130	90	90[a]	44	–[d]
111	50.1	–[d]	51.2	–[d]
041[e]	51.4	–[d]	90	90[a]
060	90	90[a]	90	–[d]

[a] Measured on Fig. 1.
[b] Measured on Fig. 4a.
[c] Unresolved peak.
[d] Too weak to be measured but qualitatively consistent with the results published in Ref. [11].
[e] Dean et al. Ref. [11] identified this reflection as (13−1). The (041) and (13 − 1) reflections are very close [15] but only the (041) indexing is consistent with the model.

Table 4
Calculated and measured azimuthal angles of the maximum of diffracted intensity (*hkl*) with respect to the fiber axis, after saturation of the lamellar rotation. The measurements were made on the histograms calculated from the upper half of Fig. 4e. The calculation was based on the lamellar twist model described in the text

	Parent lamellae		Daughter lamellae	
hkl	Calculated angle (°)	Measured angle (°)	Calculated angle (°)	Measured angle (°)
110	72.7	~ 80[a]	68	~ 80[a]
040	6	6	6	6
130	47.1	50 (41)[b]	46.4	50 (41)[b]
111	74.6	~ 80[a]	75.1	~ 80[a]
041	40.3	–[c]	39.6	–[c]

[a] Unresolved peak.
[b] The azimuthal angles for the 2 arcs are not the same.
[c] Too weak to be measured.

morphology of the α iPP tc layer is not uniform in the direction transverse to the fiber axis but changes gradually from one conformation to the other. The change is complete at a distance of approximately 25 μm from the fiber. The nature of the passage depends on the two end conformations, and model building is complicated by the presence of two populations of lamellae. The model for distances greater than 25 μm from the fiber is unambiguous due to the superposition of the X-ray diffraction patterns of parent and daughter lamellae. However, the morphology close to the nucleation site is less certain. We have presented one model (Fig. 5a) which is consistent with the X-ray diffraction data and is also physically reasonable; nevertheless the merits of a second model should be explored. In Fig. 1, the meridional (110) arcs which Dean [11] and we have identified as being generated by the daughter lamellae, are more intense than the corresponding equatorial arcs induced by the parent lamellae. The relative intensity of the arcs is not sufficient to determine the relative sizes of the two populations of lamellae, however one may expect that there are more parent than daughter lamellae. We may analyze the consequence of inverting the identification of the parent and daughter lamellae. In such a model, close to the fiber, the crystallite a^*-axis in parent lamellae and the c^*-axis of daughter lamellae would be parallel to the fiber. The a^*c^* plane of the parent lamellae would be in contact with the fiber surface. The passage from this conformation to the final one would occur by a bending of the parent lamellae around the parent *c*-axis (sheaf-like structure). The azimuthal angles of the reciprocal lattice vectors for the parent lamellae with respect to the fiber axis are listed in Table 5. The similarity of the calculated angles presented in Tables 3 and 5 does not permit us to distinguish between the two models even for the (111) reflection: the 9° difference is not conclusive because the arcs are weak and diffuse. Nevertheless the first model is still favored; α iPP is more likely to grow epitaxially on the fiber surface. We have not found in the literature evidence of lamellar twisting in pure spherulitic α iPP but β iPP lamellae may twist under certain thermal conditions. Interestingly, when the β phase is melted and recrystallized in α iPP, the twisting remains [16]. Lamellar twisting about the growth direction has already been shown for transcrystalline polyethylene [1] but this is consistent with what was already known to exist in spherulitic polyethylene. Finally, micromechanical experiments performed in the α iPP tc layer at different distances from the fiber support the model of twisting of the lamellae around its growth direction [17]. Due to the high density of nucleation sites at the fiber surface the driving force for rotation may be the crowding of the lamellae close to the fiber. It should be noted that X-ray diffraction measurements performed on β and γ iPP transcrystallinity, where there are no daughter lamellae, have not demonstrated any lamellar twisting [18].

Table 5
Calculated and measured azimuthal angles of the maximum of diffracted intensity (*hkl*) of the parent lamellae with respect to the fiber, close to the fiber surface. The measurements were made on the histograms calculated from Fig. 1 and from the upper half of Fig. 4a. The calculation was based on the lamellar sheaf model described in the text

hkl	Calculated angle (°)	Measured angle (°)
110	17.4	~0[a,b,c]
040	90	90[a,b]
130	43.2	–[d]
111	50.5	–[d]
041	90	90[a]
060	90	–[d]

[a] Measured on Fig. 1.
[b] Measured on Fig. 4a.
[c] Unresolved peak.
[d] Too weak to be measured.

5. Conclusions

The X-ray diffraction experiments on aramid/α isotactic polypropylene microcomposites described here demonstrate

a dramatic change in the orientation of the polypropylene lamellae as they grow radially outwards from the fiber surface. The data support a 90° twist of the parent lamellae about the a^*-axis occuring within a distance of about 25 μm and with a pitch which is not uniform. Subsequently, the lamellae grow without further twisting. This 90° twist seems to be a general result since it has been reproduced for different fibers, isotactic polypropylene matrices and crystallization temperatures. Our result is particularly surprising since in spherulitic polypropylene the lamellae appear to grow radially and straight from the center of the spherulites.

Acknowledgements

H.D.W. is the recipient of the Livio Norzi Professorial Chair. This project was supported by a grant from the MINERVA Foundation, and by the Israel Ministry of Science. The authors would like to thank Bill Lamberti of ExxonMobil Corporate Strategic Research for his expert scanning electron microscopy imaging and micrographs.

References

[1] Klein N, Marom G, Wachtel E. Polymer 1996;37:5493.
[2] Stern T, Wachtel E, Marom G. J Polym Sci Part B: Polym Phys 1997;35:2429.
[3] Chen EJH, Hsiao BS. Polym Eng Sci 1992;32:280.
[4] Nuriel H, Klein N, Marom G. Comp Sci Technol 1999;59:1685.
[5] Lovinger AJ. J Polym Sci Part B: Polym Phys 1983;21:97.
[6] Padden Jr JF, Keith HD. J Appl Phys 1966;37:4013.
[7] Lustiger A, Marzinsky CN, Mueller RR, Wagner HD. J Adhes 1995;53:1.
[8] Varga J, Karger-Kocsis J. Polymer 1995;36:4877.
[9] Assouline E, Fulchiron R, Gérard J-F, Wachtel E, Wagner HD, Marom G. J Polym Sci Part B: Polym Phys 1999;37:2534.
[10] Amitay-Sadovsky E, Cohen SR, Wagner HD. Appl Phys Lett 1999;74:2966.
[11] Dean DM, Rebenfeld L, Register A, Hsiao BS. J Mater Sci 1998;33:4797.
[12] Wagner HD, Steenbakkers LW. J Mater Sci 1989;24:3956.
[13] Bassett DC, Olley RH. Polymer 1984;25:935.
[14] Kakudo M, Kasai N. X-Ray diffraction by polymers. Amsterdam: Elsevier, 1972. p. 231.
[15] Samuels RJ, Yee RY. J Polym Sci Part A-2 1972;10:385.
[16] Padden Jr JF, Keith HD. J Appl Phys 1959;30:1479.
[17] Amitay-Sadovsky E, Cohen SR, Wagner HD. Macromolecules 2001;34:1252.
[18] Assouline E. Unpublished results.